Automatica 53 (2015) 320–328

Contents lists available at ScienceDirect

Automatica

journal homepage: www.elsevier.com/locate/automatica

Bounded droop controller for parallel operation of inverters☆

George C. Konstantopoulos [a,1], Qing-Chang Zhong [a,b], Beibei Ren [c], Miroslav Krstic [d]

[a] Department of Automatic Control and Systems Engineering, The University of Sheffield, Sheffield, S1 3JD, UK
[b] Department of Electrical and Computer Engineering, Illinois Institute of Technology, Chicago, IL 60616, USA
[c] Department of Mechanical Engineering, Texas Tech University, Lubbock, TX 79409, USA
[d] Department of Mechanical and Aerospace Engineering, University of California, San Diego, CA 92093, USA

ARTICLE INFO

Article history:
Received 6 November 2013
Received in revised form
19 November 2014
Accepted 21 December 2014
Available online 8 February 2015

Keywords:
Droop control
Non-linear systems
Stability
Parallel operation of inverters
Proportional load sharing

ABSTRACT

In this paper, the stability of parallel-operated inverters in the sense of boundedness is investigated. At first, the non-linear model of parallelled inverters with a generic linear or non-linear load is obtained by using the generalised dissipative Hamiltonian structure and then the robust droop controller, recently proposed in the literature for parallel operation of inverters, is implemented in a way to produce a bounded control output. The proposed controller is called the bounded droop controller (BDC). It introduces a zero-gain property and can guarantee the boundedness of the closed-loop system solution. Therefore, for the first time, the closed-loop stability in the sense of boundedness is guaranteed for parallelled inverters feeding generic non-linear/linear loads. The controller structure is further improved to increase its robustness with respect to initial conditions, numerical errors or external disturbances while maintaining the stability property. Moreover, the controller is tuned to avoid any possible limit cycles in the voltage dynamics. Real-time simulation results for two single-phase inverters operated in parallel loaded with a non-linear load are presented to verify the effectiveness of the proposed BDC.

1. Introduction

The penetration of renewable energy sources into electrical networks has increased in the last decades due to environmental, technical and economical reasons. Their integration is accomplished by using suitable power electronic devices (inverters), thus forming distributed generation units. The integration of renewable sources along with energy storage devices and local loads form a microgrid, which has been extensively studied in the literature (Guerrero, Chandorkar, Lee, & Loh, 2013; Guerrero, Loh, Lee, & Chandorkar, 2013; Guerrero, Vasquez, Matas, Castilla, & de Vicuna, 2009; Iyer, Belur, & Chandorkar, 2010; Weiss, Zhong, Green, & Liang, 2004; Zhong & Hornik, 2013). In microgrids, due to the limited availability of high current power electronic devices, inverters are often operated in parallel. In order to avoid circulating currents among the inverters, the droop control method (Barklund, Pogaku, Prodanovic, Hernandez-Aramburo, & Green, 2008; Guerrero, Chandorkar et al., 2013; Guerrero, Loh et al., 2013; Guerrero, Vasquez, Matas, Garcia de Vicuna, & Castilla, 2011), which does not require any external communication mechanism among the inverters (Chandorkar, Divan, & Adapa, 1993; Tuladhar, Jin, Unger, & Mauch, 1997), is often adopted. However, secondary control is often used to restore the microgrid voltage and frequency to the desired level (Guerrero, Chandorkar et al., 2013; Guerrero et al., 2009, 2011).

One of the main issues in microgrid operation is the accurate power sharing among the parallelled inverters in accordance to their power ratings, which should be maintained in both grid-connected and stand-alone operation. Especially in the stand-alone mode, load sharing according to each inverter capacity under different operating conditions is a challenging task (Sao & Lehn, 2005), which is usually achieved using droop control techniques. However, conventional droop controllers introduce inherent limitations in accurate real and reactive power sharing as noted in Zhong (2013) and Zhong and Hornik (2013). Additionally, the inverter output impedance plays a key role in accurate load sharing, since inverters equipped with the conventional droop control are

☆ The financial support from the EPSRC, UK, under Grant No. EP/J01558X/1 is greatly appreciated. The material in this paper was partially presented at the 2014 American Control Conference 2014, June 4–6, 2014, Portland, OR, USA. This paper was recommended for publication in revised form by Associate Editor Huaguang Zhang under the direction of Editor Toshiharu Sugie.

E-mail addresses: g.konstantopoulos@sheffield.ac.uk (G.C. Konstantopoulos), zhongqc@ieee.org (Q.-C. Zhong), beibei.ren@ttu.edu (B. Ren), krstic@ucsd.edu (M. Krstic).

[1] Tel.: +44 114 222 6080; fax: +44 114 22 25683.

http://dx.doi.org/10.1016/j.automatica.2015.01.012
0005-1098/

required to have the same per-unit output impedance (Guerrero, de Vicuna, Matas, Castilla, & Miret, 2005). Therefore, recently, several control designs have been proposed in order to achieve accurate power sharing among the inverters (Guerrero et al., 2006; Guerrero, Matas, de Vicuna, Castilla, & Miret, 2007; Li & Kao, 2009; Majumder, Chaudhuri, Ghosh, Ledwich, & Zare, 2010; Mohamed & El-Saadany, 2008; Zhong, 2013). Among these techniques, the robust droop controller (RDC) proposed in Zhong (2013) has been proven to achieve accurate load sharing even if numerical computational errors, disturbances, noises, parameter drifts and component mismatches occur.

Although a lot of research has been done in the field of load sharing, the stability properties of the proposed techniques have not been adequately exploited. Most of the stability analysis has been focused on small-signal modelling and linearisation methods (Coelho, Cortizo, & Garcia, 2002; Majumder et al., 2010; Marwali, Jung, & Keyhani, 2007; Mohamed & El-Saadany, 2008), which are only valid around a specific equilibrium point (local stability). Several conditions of the local exponential stability for frequency droop control are exploited in Simpson-Porco, Dörfler, and Bullo (2013), where however fixed or bounded voltage magnitudes and a purely inductive network are considered. Due to the non-linear structure of the droop controller, it becomes obvious that the non-linear stability analysis is essential for investigating the behaviour of parallel inverters. Recently the $\mathcal{L}_\infty$ stability of the conventional droop control has been proven in Schiffer, Ortega, Astolfi, Raisch, and Sezi (2014) where asymptotic stability of lossless microgrids is also achieved. In this work, the Kron-reduced network is considered and instantaneous frequency regulation is assumed for the analysis. It should be noted that the Kron-reduced network approach considers all loads in the linear form. Non-linear load dynamics can be suitably investigated only using the inverter currents model.

To the best of the authors' knowledge, the non-linear stability of a robust droop control technique, which achieves accurate load sharing, independently from the type of the load (linear or non-linear) has not been solved yet. In this paper, two parallel single-phase inverters feeding a local load are considered. The load is given in the generalised dissipative Hamiltonian form, which represents the general case of a power electronic-driven dynamic system (Konstantopoulos & Alexandridis, 2013; Ortega, Loria, Nicklasson, & Sira-Ramirez, 1998). For this system, the robust droop controller proposed in Zhong (2013) can be considered, since it is proven to achieve the most robust performance and introduces a dynamic voltage droop opposed to the conventional droop controllers. Particularly, in the present work, in order to analyse the stability of inverters operated in parallel, the RDC is implemented in a way to ensure that the control input stays within a predefined range, without changing the main concept of the initial control design. The controller performance is extensively analysed using non-linear Lyapunov methods and is proven to achieve a bounded performance. Using $\mathcal{L}_\infty$ stability analysis and the small-gain theorem (Khalil, 2001), the first proof of stability in the sense of boundedness is presented for the non-linear closed-loop system using the important zero-gain property of the proposed controller. Further investigation of the controller structure leads to the final form of the proposed bounded droop controller (BDC) which is robust to external disturbances and guarantees the desired performance. This represents a significant superiority with respect to the existing techniques since robust accurate load sharing is achieved with a guaranteed stability for a general load case using a dynamic droop controller. Extensive real-time simulation results for two inverters in parallel operation with a non-linear load are illustrated to verify the effectiveness of the proposed BDC compared to the RDC using an OPAL-RT real-time digital simulator.

The paper is organised as follows. In Section 2, the dynamic model of the system consisting of two single-phase inverters and a load is obtained along with its properties and an overview of the robust droop controller is presented. In Section 3, the bounded droop controller is proposed and its performance is investigated. Furthermore, the boundedness of the closed-loop system is proven using non-linear analysis. The controller structure is further improved to increase its robustness with respect to computational errors or disturbances and guarantee a desired operation. In Section 4, extensive real-time simulation results are provided to certify the effectiveness of the proposed bounded control scheme and, finally, in Section 5, some conclusions are drawn.

2. Parallel operation of inverters

2.1. System modelling

Fig. 1 represents the schematic diagram of two single-phase inverters connected in parallel feeding a common load. An LC filter is assumed at the output of each inverter where L_1, L_2 and C_1, C_2 are the filter inductances and capacitances respectively for each inverter. In practice, each inductor and capacitor introduces parasitic resistances represented as R_1 and R_2 in series with the inductors (typically very small) and r_{C1} and r_{C2} in parallel with the capacitors (typically very large). Variables v_{r1}, v_{r2} and i_1, i_2 are the inverter output voltages and currents, respectively, while v_o and i_L are the load voltage and current, respectively. The filter capacitors along with the parasitic resistances can be regarded as a part of the load and therefore, C_1, C_2, r_{C1} and r_{C2} can represent some of the load characteristics as well (Zhong, 2013; Zhong & Hornik, 2013). The dynamic equations of the system are

$$\begin{aligned} L_1\frac{di_1}{dt} &= -R_1 i_1 - v_o + v_{r1},\\ L_2\frac{di_2}{dt} &= -R_2 i_2 - v_o + v_{r2},\\ (C_1+C_2)\frac{dv_o}{dt} &= i_1 + i_2 - \frac{r_{C1}+r_{C2}}{r_{C1}r_{C2}}v_o - i_L. \end{aligned} \tag{1}$$

Although a lot of research has been done for linear loads (resistive, resistive–inductive), in a typical application the load is usually non-linear. This increases the difficulty of the control design and the analysis. However, since most of the loads are fed by power electronic devices (power converters), by using average analysis (Ortega et al., 1998), the load can be represented by the generalised dissipative Hamiltonian form Konstantopoulos and Alexandridis (2013) and Ortega et al. (1998)

$$M\dot{w} = (J(w,\mu) - R)\,w + Gv_o, \tag{2}$$

where $w = \begin{bmatrix} i_L & w_1 & w_2 \dots & w_{m-1}\end{bmatrix}^T \in \mathcal{R}^m$ represents the states of the load and μ is a bounded vector in a closed set which describes the duty-ratio signals of the converters. Matrix M is constant and positive definite, J is skew-symmetric, R is constant and positive definite and $G = \begin{bmatrix}1 & 0_{1\times(m-1)}\end{bmatrix}^T$. For the load equation (2), the load voltage can be considered as an input to the load system (in fact this is usually the case when for example a voltage source device is connected at the inverter's output). It should also be noted that all non-linearities of the load and the bounded duty-ratio signals μ are restricted into the skew-symmetric matrix J. This is a common issue in power systems, especially for power converter-fed loads (Karagiannis, Mendes, Astolfi, & Ortega, 2003; Konstantopoulos & Alexandridis, 2013; Ortega et al., 1998). As a result, the complete plant system can be written into the generalised dissipative Hamiltonian form

$$\tilde{M}\dot{\tilde{x}} = \left(\tilde{J}(\tilde{x},\mu) - \tilde{R}\right)\tilde{x} + \tilde{G}u, \tag{3}$$

where the state vector is $\tilde{x} = \begin{bmatrix} i_1 & i_2 & v_o & w^T\end{bmatrix}^T$, the input vector is $u = \begin{bmatrix} v_{r1} & v_{r2}\end{bmatrix}^T$ and matrices $\tilde{M}, \tilde{J}$ and $\tilde{R}$ as defined below retain

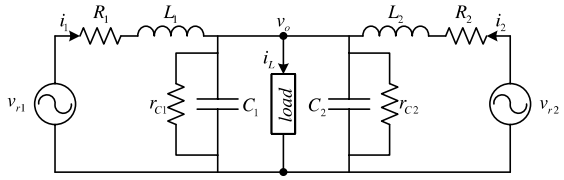

Fig. 1. Schematic diagram of parallel-operated inverters.

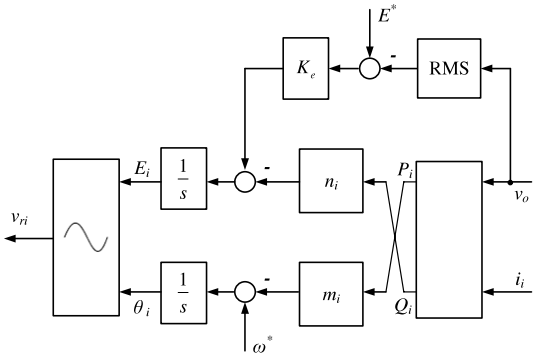

Fig. 2. Robust droop controller (RDC) (Zhong & Hornik, 2013).

the properties already mentioned:

$$\tilde{M} = \begin{bmatrix} L_1 & 0 & 0 & 0_{1\times m} \\ 0 & L_2 & 0 & 0_{1\times m} \\ 0 & 0 & C_1+C_2 & 0_{1\times m} \\ 0_{m\times 1} & 0_{m\times 1} & 0_{m\times 1} & M \end{bmatrix},$$

$$\tilde{J} = \begin{bmatrix} 0 & 0 & -1 & 0 & 0_{1\times(m-1)} \\ 0 & 0 & -1 & 0 & 0_{1\times(m-1)} \\ 1 & 1 & 0 & -1 & 0_{1\times(m-1)} \\ 0 & 0 & 1 & 0 & J_{12} \\ 0_{(m-1)\times 1} & 0_{(m-1)\times 1} & 0_{(m-1)\times 1} & -J_{12}^T & J_{22} \end{bmatrix},$$

$$\tilde{R} = \begin{bmatrix} R_1 & 0 & 0 & 0_{1\times m} \\ 0 & R_2 & 0 & 0_{1\times m} \\ 0 & 0 & \dfrac{r_{C1}+r_{C2}}{r_{C1}r_{C2}} & 0_{1\times m} \\ 0_{m\times 1} & 0_{m\times 1} & 0_{m\times 1} & R \end{bmatrix},$$

$$\tilde{G} = \begin{bmatrix} 1 & 0 & 0_{1\times(m+1)} \\ 0 & 1 & 0_{1\times(m+1)} \end{bmatrix}^T,$$

where $J = \begin{bmatrix} 0 & J_{12} \\ -J_{12}^T & J_{22} \end{bmatrix}$ with J_{12} and J_{22} being $1\times(m-1)$ and $(m-1)\times(m-1)$ matrices, respectively.

It should be noted that the plant system (3) is a non-linear bounded input bounded output (BIBO) stable system, which accurately describes a generic non-linear load. The output vector can be the whole state vector or part of it.

2.2. Accurate power sharing

The main issue in parallel operation of inverters is to achieve accurate power sharing of the inverters according to their power ratings. This can be solved by using the robust droop control (RDC) technique proposed in Zhong (2013), which, as shown in Fig. 2 for each inverter $i \in \{1, 2\}$, takes the form

$$\dot{E}_i = K_e\left(E^* - V_o\right) - n_i Q_i \tag{4}$$

$$\dot{\theta}_i = \omega^* - m_i P_i \tag{5}$$

where E_i and θ_i are the RMS value and the phase angle of the ith inverter output voltage; E^* and ω^* are the rated voltage and angular frequency, respectively; V_o represents the RMS voltage of the load and P_i, Q_i are the real and reactive power delivered at the load by the ith inverter. Control parameters K_e, n_i and m_i are suitably determined by the desired voltage and frequency droop ratio (Zhong, 2013). Thus, the control input (inverter output voltage) is given in the form

$$v_{ri} = \sqrt{2}E_i \sin(\theta_i). \tag{6}$$

The controller and the dynamics are non-linear, since the RMS load voltage is a non-linear function of v_o, i.e. $V_o(v_o)$, and the real and reactive powers are also non-linear functions of v_o and i_i, i.e. $P_i(v_o, i_i)$, $Q_i(v_o, i_i)$. This makes it very difficult to directly investigate the stability of the closed-loop system. Several researchers have recently proved the stability of the inverter-based systems but only when the conventional droop controller is used and under the assumption of a linear load (Schiffer et al., 2014; Simpson-Porco et al., 2013). However, the conventional droop controller is static while the voltage droop of the RDC given in (4) is dynamic. This significantly increases the difficulty of proving stability. To the best of the authors' knowledge, the stability analysis using the robust droop controller which achieves accurate power sharing for a general type of load has not yet been exploited.

3. Controller design and analysis

3.1. Bounded droop controller (BDC)

As shown in the previous section, the robust droop controller (4)–(5) contains two parts: controlling the RMS voltage E_i and the angular frequency $\dot{\theta}_i$. Then a sinusoidal signal with the angle θ_i is created and combined with E_i in order to finally form the control law (6).

In this paper, to facilitate the stability analysis of the inverter-based system using the robust droop controller, (4)–(6) are implemented in the following form, while keeping the main idea intact:

$$v_{ri} = \sqrt{2}E_i z_i \tag{7}$$

with the dynamics for the RMS voltage given as

$$\dot{E}_i = \left(K_e\left(E^* - V_o\right) - n_i Q_i\right) cE_{qi}, \tag{8}$$

$$\dot{E}_{qi} = -\left(K_e\left(E^* - V_o\right) - n_i Q_i\right) cE_i, \tag{9}$$

where c is a positive constant, and the dynamics of the angular frequency given as

$$\dot{z}_i = \left(\omega^* - m_i P_i\right) z_{qi}, \tag{10}$$

$$\dot{z}_{qi} = -\left(\omega^* - m_i P_i\right) z_i. \tag{11}$$

It should be mentioned that two extra state variables, E_{qi} and z_{qi}, are added to represent the dynamics of the RMS voltage and the angular frequency respectively, while the initial theory of the robust droop controller is maintained. It becomes clear from (8)–(9) and (10)–(11) that the controller is represented by a non-linear double integrator scheme, thus acting as an oscillator.

In order to understand the control performance, the RMS voltage dynamics (8)–(9) are investigated at first, by considering the Lyapunov function candidate

$$W_i(t) = E_i^2 + E_{qi}^2. \tag{12}$$

Then, taking into account (8)–(9), it results that

$$W_i(t) = W_{i0} = E_{i0}^2 + E_{qi0}^2, \quad \forall t \geq 0 \tag{13}$$

where E_{i0} and E_{qi0} are the initial values of the controller states. Eq. (13) implies that E_i and E_{qi} will move on the circumference of

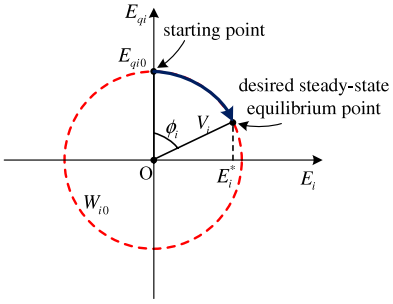

Fig. 3. Controller states of the voltage dynamics.

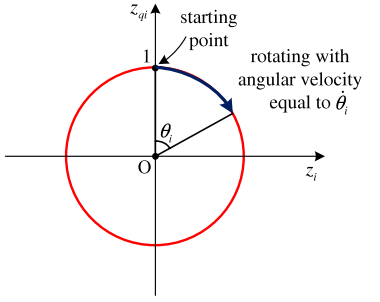

Fig. 4. Controller states of the frequency dynamics.

a circle at the origin O and radius $V_i = \sqrt{E_{i0}^2 + E_{qi0}^2}$ for all $t \geq 0$. Since in a typical load sharing application, it is desirable that each inverter starts operating from a zero output voltage, the initial conditions of the controller states can be chosen with $E_{i0} = 0$ and $E_{qi0} > 0$ in order for the states to start from a point on the E_{qi}-axis and move clockwise; see Fig. 3. The circle can be described by the transformation

$$E_i = V_i \sin \phi_i \quad \text{and} \quad E_{qi} = V_i \cos \phi_i. \tag{14}$$

Because of (8) and (9), there is

$$\dot{\phi}_i = \left(K_e \left(E^* - V_o\right) - n_i Q_i\right) c, \tag{15}$$

which is the angular velocity of the movement of the controller states E_i and E_{qi} on the circumference of the circle. Also note that the controller state variables E_i and E_{qi} will be bounded in the set $[-V_i, V_i]$ defined by their initial conditions, independently from the angular velocity (15). In practice, V_i can be chosen as the maximum allowed voltage $V_i = (1 + p) E^*$, where p is the allowed percentage over the rated voltage E^*. At the desired steady-state equilibrium, corresponding to the point $\left(E_i^*, E_{qi}^*\right)$ on the circle in Fig. 3, it holds true that (Zhong, 2013):

$$K_e \left(E^* - V_o\right) - n_i Q_i = 0. \tag{16}$$

As a result, the angular velocity $\dot{\phi}_i$ becomes zero at the steady-state equilibrium and E_i and E_{qi} will eventually stop changing and converge to the desired equilibrium.

The frequency dynamics, which represent the angular frequency of the robust droop controller (10)–(11), can be handled in the same manner. A similar transformation, with the state z_i representing the sinusoidal function $\sin(\theta_i)$ and $\dot{\theta}_i$ being the angular frequency (5) of the system, can be defined. Therefore, by considering initial conditions $z_{i0} = 0$ and $z_{qi0} = 1$, a similar analysis will show that z_i and z_{qi} move on a circle at the origin with radius equal to 1 (as implied by the initial conditions, see Fig. 4) with angular velocity $\dot{\theta}_i$.

At the desired steady-state equilibrium it holds that $\dot{\theta}_i \neq 0$, since it represents the frequency of the system (Zhong, 2013), the state variables z_i and z_{qi} will continuously move on their circle

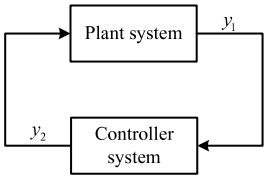

Fig. 5. Closed-loop system in feedback interconnection.

forming two functions $\sin(\theta_i)$ and $\cos(\theta_i)$ respectively. In fact, this is the purpose of the design if one directly compares (6) and (7).

It becomes obvious that since E_i and E_{qi} are bounded in the interval $[-V_i, V_i]$ and z_i and z_{qi} are also bounded in the interval $[-1, 1]$, then the inverter output voltage v_{ri}, given by (7), is bounded in the interval $\left[-\sqrt{2}V_i, \sqrt{2}V_i\right]$, thus forming a bounded droop controller (BDC).

As a result, the closed-loop system becomes

$$\dot{\bar{x}} = \begin{bmatrix} -\frac{R_1}{L_1} i_1 - \frac{1}{L_1} v_o + \frac{\sqrt{2} E_1 z_1}{L_1} \\ -\frac{R_2}{L_2} i_2 - \frac{1}{L_2} v_o + \frac{\sqrt{2} E_2 z_2}{L_2} \\ \frac{1}{C_1 + C_2} i_1 + \frac{1}{C_1 + C_2} i_2 - \frac{r_{C1} + r_{C2}}{(C_1 + C_2)\, r_{C1} r_{C2}} v_o - \frac{1}{C_1 + C_2} i_L \\ M^{-1} G v_o + M^{-1} \left(J(w, \mu) - R\right) w \\ \left(K_e \left(E^* - V_o(v_o)\right) - n_1 Q_1(v_o, i_1)\right) c E_{q1} \\ -\left(K_e \left(E^* - V_o(v_o)\right) - n_1 Q_1(v_o, i_1)\right) c E_1 \\ \left(\omega^* - m_1 P_1(v_o, i_1)\right) z_{q1} \\ -\left(\omega^* - m_1 P_1(v_o, i_1)\right) z_1 \\ \left(K_e \left(E^* - V_o(v_o)\right) - n_2 Q_2(v_o, i_2)\right) c E_{q2} \\ -\left(K_e \left(E^* - V_o(v_o)\right) - n_2 Q_2(v_o, i_2)\right) c E_2 \\ \left(\omega^* - m_2 P_2(v_o, i_2)\right) z_{q2} \\ -\left(\omega^* - m_2 P_2(v_o, i_2)\right) z_2 \end{bmatrix} \tag{17}$$

where $\bar{x} = \left[i_1 \;\; i_2 \;\; v_o \;\; w^T \;\; E_1 \;\; E_{q1} \;\; z_1 \;\; z_{q1} \;\; E_2 \;\; E_{q2} \;\; z_2 \;\; z_{q2}\right]^T$ is the closed-loop state vector.

3.2. Boundedness of the system

From the closed-loop system described in (17), it becomes obvious that the closed-loop system can be investigated as a feedback interconnection of the plant system and the controller system shown in Fig. 5.

Following (3), the plant system is given in the form

$$\tilde{M} \dot{\tilde{x}} = \left(\tilde{J}(\tilde{x}, \mu) - \tilde{R}\right) \tilde{x} + \tilde{G} y_2 \tag{18}$$

$$y_1 = \left[i_1 \quad i_2 \quad v_o\right]^T, \tag{19}$$

while the controller system is given in the form

$$\frac{d}{dt} \begin{bmatrix} E_1 \\ E_{q1} \\ z_1 \\ z_{q1} \\ E_2 \\ E_{q2} \\ z_2 \\ z_{q2} \end{bmatrix} = \begin{bmatrix} A_1(y_1) & 0_{2\times2} & 0_{2\times2} & 0_{2\times2} \\ 0_{2\times2} & A_2(y_1) & 0_{2\times2} & 0_{2\times2} \\ 0_{2\times2} & 0_{2\times2} & A_3(y_1) & 0_{2\times2} \\ 0_{2\times2} & 0_{2\times2} & 0_{2\times2} & A_4(y_1) \end{bmatrix} \begin{bmatrix} E_1 \\ E_{q1} \\ z_1 \\ z_{q1} \\ E_2 \\ E_{q2} \\ z_2 \\ z_{q2} \end{bmatrix}, \tag{20}$$

$$y_2 = \begin{bmatrix} \sqrt{2} E_1 z_1 \\ \sqrt{2} E_2 z_2 \end{bmatrix}, \tag{21}$$

with

$$A_1(y_1) = \begin{bmatrix} 0 & \dot{\phi}_1 \\ -\dot{\phi}_1 & 0 \end{bmatrix}, \quad A_2(y_1) = \begin{bmatrix} 0 & \dot{\theta}_1 \\ -\dot{\theta}_1 & 0 \end{bmatrix},$$
$$A_3(y_1) = \begin{bmatrix} 0 & \dot{\phi}_2 \\ -\dot{\phi}_2 & 0 \end{bmatrix}, \quad A_4(y_1) = \begin{bmatrix} 0 & \dot{\theta}_2 \\ -\dot{\theta}_2 & 0 \end{bmatrix}.$$

In the feedback interconnection shown in Fig. 5, even if the plant system is BIBO, it is not guaranteed that the controller output will be bounded. This makes the stability analysis of the closed-loop system very complicated and represents the reason why the conventional droop control cannot guarantee global bounded results. This problem can now be solved using the BDC.

Proposition 1. *The closed-loop system of Fig. 5 with the plant system given by (18)–(19) and the controller system given by (20)–(21) is stable in the sense of boundedness, i.e., the closed-loop system solution $\bar{x}(t)$ is bounded for all $t \geq 0$.*

Proof. The main purpose is to prove boundedness of the closed-loop system solution; thus the analysis will be conducted in the $\mathcal{L}_\infty$ space. Investigate initially the plant system dynamics given by (18) or equivalently (3) by considering the Lyapunov function

$$V(\tilde{x}) = \frac{1}{2}\tilde{x}^T \tilde{M}\tilde{x}. \tag{22}$$

The time derivative of V is

$$\begin{aligned} \dot{V} &= -\tilde{x}^T \tilde{R}\tilde{x} + \tilde{x}^T \tilde{G}u \\ &= -R_1 i_1^2 - R_2 i_2^2 - \frac{r_{C1}+r_{C2}}{r_{C1}r_{C2}} v_o^2 - w^T R w + \tilde{x}^T \tilde{G}u \\ &\leq -(1-a)\lambda_{\min}\left(\tilde{R}\right)\|\tilde{x}\|_2^2, \\ &\quad \forall \|\tilde{x}\|_2 \geq \frac{1}{\min\left\{R_1, R_2, \frac{r_{C1}+r_{C2}}{r_{C1}r_{C2}}, \lambda_{\min}(R)\right\} a}\|u\|_2 \end{aligned} \tag{23}$$

where $0 < a < 1$ and $\lambda_{\min}(R)$ is the minimum eigenvalue of the constant positive definite matrix R. Since the Lyapunov function V is radially unbounded, the inequality (23) implies that the plant system is input-to-state stable (ISS) (Khalil, 2001). Since the bounded vector μ does not affect the analysis, there exist non-negative constants γ_{plant} and β_{plant} such that

$$\|y_{1\tau}\|_{\mathcal{L}_\infty} \leq \gamma_{plant}\|y_{2\tau}\|_{\mathcal{L}_\infty} + \beta_{plant} \tag{24}$$

for all $y_2 \in \mathcal{L}^2$ and $\tau \in [0, \infty)$ and as a result the plant system is finite-gain $\mathcal{L}_\infty$ stable with gain γ_{plant} (Khalil, 2001), which actually means that the plant system is BIBO.

Now, by investigating the controller system (20)–(21), due to the matrix diagonal structure, one can investigate every controller subsystem $(E_1 - E_{q1}, z_1 - z_{q1}, E_2 - E_{q2}, z_2 - z_{q2})$ separately where it is considered that $y_1 \in \mathcal{L}^3$.

According to the analysis described in Section 3.1, E_i and E_{qi} are bounded in the set $[-V_i, V_i]$ and z_i and z_{qi} are bounded in the set $[-1, 1]$ for every bounded input y_1, i.e. it can be easily proven that there exists a non-negative constant $\beta_{control}$ such that:

$$\|y_{2\tau}\|_{\mathcal{L}_\infty} = \sqrt{2}\left\|\begin{matrix} E_{1\tau}z_{1\tau} \\ E_{2\tau}z_{2\tau} \end{matrix}\right\|_{\mathcal{L}_\infty} \leq \beta_{control}. \tag{25}$$

The controller system (20)–(21) is also finite-gain $\mathcal{L}_\infty$ stable with gain $\gamma_{control} = 0$, because (25) holds true independently from the input y_1. Then, according to the small-gain theorem (Khalil, 2001), it holds true that $\gamma_{plant}\gamma_{control} < 1$. Since no other external inputs are applied to the system, as shown in Fig. 5, the closed-loop system solution is bounded. □

As a result, the zero-gain property of the BDC guarantees boundedness of the closed-loop system solution independently from the plant parameters. This provides a generic solution for controlling inverters operated in parallel. Additionally, the BDC can also guarantee a maximum bound for the inverter output voltage as proven in the previous subsection, thus protecting each inverter from violating its technical limits.

In practice, the measuring and processing of the real and reactive powers P_i and Q_i are obtained through low-pass filters (Coelho et al., 2002). Low-pass filters are always finite-gain $\mathcal{L}_\infty$ stable with a finite gain γ_{filter} and they can be represented as a series connection of the controller system in the feedback loop in Fig. 5. Since the series connection of two $\mathcal{L}_\infty$ stable systems is also $\mathcal{L}_\infty$ stable with finite gain $\gamma_{filter}\gamma_{control}$ and the controller has zero gain, then obviously the stability analysis is not affected by these filters.

Remark 2. Since the closed-loop system is now bounded, the currents of the inverters are bounded. Moreover, the real power and the reactive power are bounded as well, which means the frequencies are bounded as well.

3.3. Improvement of the controller robustness

The BDC dynamics given in (8)–(9) and (10)–(11) can be rewritten in the following matrix forms:

$$\begin{bmatrix} \dot{E}_i \\ \dot{E}_{qi} \end{bmatrix} = \begin{bmatrix} 0 & \dot{\phi}_i \\ -\dot{\phi}_i & 0 \end{bmatrix} \begin{bmatrix} E_i \\ E_{qi} \end{bmatrix} \tag{26}$$

$$\begin{bmatrix} \dot{z}_i \\ \dot{z}_{qi} \end{bmatrix} = \begin{bmatrix} 0 & \dot{\theta}_i \\ -\dot{\theta}_i & 0 \end{bmatrix} \begin{bmatrix} z_i \\ z_{qi} \end{bmatrix} \tag{27}$$

with $\dot{\phi}_i$ and $\dot{\theta}_i$ given in (15) and (5) respectively. This forms two non-linear oscillators.

From the analysis presented in Section 3.1, it is clear that the proposed scheme depends on the initial conditions. The question is whether the controller can be effective if an error/noise that changes the initial conditions occurs, or during the application the states are disturbed from the desired circle due to numerical errors, etc. To overcome these problems, the zero diagonal terms of (26) and (27) can be replaced with suitable terms to increase the robustness of the BDC, without changing the purpose of the design or the stability analysis. The new voltage dynamics is designed as

$$\begin{bmatrix} \dot{E}_i \\ \dot{E}_{qi} \end{bmatrix} = \begin{bmatrix} -k_E\left(E_i^2 + E_{qi}^2 - V_i^2\right) & \dot{\phi}_i \\ -\dot{\phi}_i & -k_E\left(E_i^2 + E_{qi}^2 - V_i^2\right) \end{bmatrix} \begin{bmatrix} E_i \\ E_{qi} \end{bmatrix} \tag{28}$$

with k_E being a positive constant and V_i representing the radius of the desired circle as already imposed in (14). In the same manner, the angular frequency dynamics is designed as

$$\begin{bmatrix} \dot{z}_i \\ \dot{z}_{qi} \end{bmatrix} = \begin{bmatrix} -k_z\left(z_i^2 + z_{qi}^2 - 1\right) & \dot{\theta}_i \\ -\dot{\theta}_i & -k_z\left(z_i^2 + z_{qi}^2 - 1\right) \end{bmatrix} \begin{bmatrix} z_i \\ z_{qi} \end{bmatrix} \tag{29}$$

with k_z being again a positive constant.

In order to understand the importance of the terms added, the voltage dynamics (28) can be investigated by considering the same Lyapunov function as given in (12), of which the time derivative is

$$\dot{W}_i(t) = -2k_E\left(E_i^2 + E_{qi}^2 - V_i^2\right)\left(E_i^2 + E_{qi}^2\right). \tag{30}$$

It makes the desired circle with radius equal to V_i as an attractive circle. When E_i and E_{qi} are outside of the circle, the derivative of the Lyapunov function is negative and when they are inside the circle the derivative is positive. This means that even if E_i and E_{qi} are disturbed at any time (and for any reason) from moving on the circumference of the circle, they will eventually return to their desired trajectory, as shown in Fig. 6. The initial conditions E_{i0} and

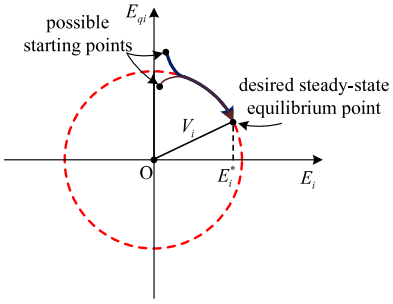

Fig. 6. Attractiveness of the controller states to the desired circle.

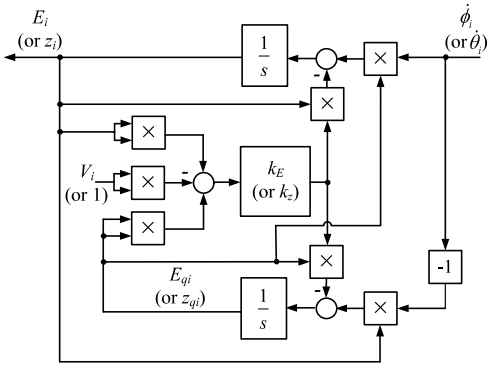

Fig. 7. Attractive oscillator.

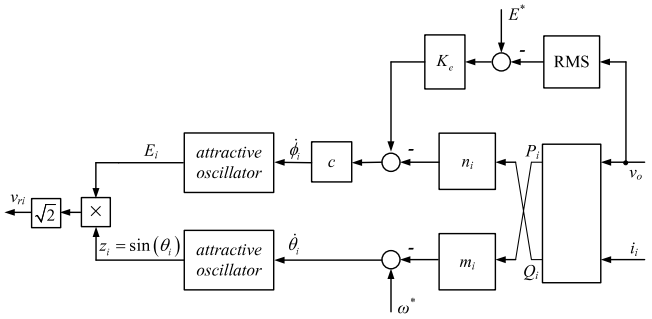

Fig. 8. Bounded droop controller (BDC).

E_{qi0} can now be any values other than 0 simultaneously. A similar analysis holds true for the frequency dynamics (29) as well. The parameters k_E and k_z determine the rate of attractiveness and can be chosen as reasonably large values. As a result, (28) and (29) each represent an attractive oscillator and can be implemented as shown in Fig. 7. The resulting BDC is shown in Fig. 8.

It is worth noting that, after adding the extra terms, the proposed controller is still finite-gain $\mathcal{L}_\infty$ stable with zero gain. This can be easily seen from (30), which implies that E_i and E_{qi} are bounded independently from the input of the system (it can be proven by contradiction). Therefore, the stability analysis described in the previous section still holds true in this case as well. The same analysis holds for z_i and z_{qi}. It should be noted that in order to avoid large transient performance, the initial conditions should be chosen as discussed in Section 3.1. The addition of the diagonal terms just increases the robustness to measuring and computational errors in order to guarantee that the controller states will definitely move on the desired circle.

3.4. Excluding possible limit cycles in the voltage dynamics

Although the boundedness of the voltage is guaranteed for any positive c, it is possible during the transient process or due to external disturbances for the voltage trajectory to pass the equilibrium point and force E_i and E_{qi} to continuously move around W_{i0}, which results in a limit cycle behaviour. To overcome this problem, the parameter c can be tuned according to the controller state variable E_{qi} as

$$c = \frac{E_{qi}}{\left(E_{qi}^*\right)^2} = \frac{E_{qi}}{V_i^2 - \left(E_i^*\right)^2} = \frac{E_{qi}}{(1+p)^2\left(E^*\right)^2 - \left(E_i^*\right)^2}. \tag{31}$$

In this case, c is time-varying and is a linear function of the state E_{qi}, which means it does not affect the stability analysis. With this c, it is clear that $cE_{qi}^* = 1$ near the steady state and that the BDC approximates the behaviour of the RDC by comparing equation (4) of the RDC with the first dynamic equation (8) of the BDC during the steady state. If E_i and E_{qi} pass the equilibrium point and try to reach the horizontal axis, i.e., $E_i \to V_i$ and $E_{qi} \to 0$, then

$$\dot{\phi}_i \to 0$$

independently from the value of $K_e\left(E^* - V_o\right) - n_i Q_i$, according to (15) and (31). Therefore, E_i and E_{qi} will slow down until the system reacts, increases the power and changes the sign of $\dot{\phi}_i$, which forces the states to eventually converge to the desired equilibrium. In the worst case, if there is no voltage equilibrium between 0 and V_i, then E_i and E_{qi} would stop at $E_i = V_i$ and $E_{qi} = 0$, respectively. This avoids any limit-cycle behaviour. As a result, a voltage value between 0 and V_i is the only positive limit set for the voltage dynamics inside the bounded range and the system will eventually converge to it Khalil (2001).

In practice, since at the beginning E_{qi} is initially large and starts decreasing as E_i and E_{qi} move on the circle, then c is initially large and the BDC acts faster than the RDC. Hence, the BDC would improve the transient performance of the system, resulting in a faster convergence to the desired equilibrium. Moreover, as noted in Zhong (2013), for a suitable K_e, the load voltage drop can be very small and therefore $V_o \approx E^*$. As a result, it can be assumed that $E_i^* \approx E^*$ and the parameter c from (31) can be simplified and tuned as

$$c = \frac{E_{qi}}{p\,(p+2)\left(E^*\right)^2}. \tag{32}$$

4. Validation with real-time simulations

In order to verify the BDC operation, two single-phase inverters operated in parallel are considered and real-time simulation results for both the BDC and the RDC, as proposed in Zhong (2013), are provided for comparison using the real-time digital simulation (RTDS) system of OPAL-RT. Each inverter is powered by a 400 V DC voltage source and the power ratings are $S_1 = 1$ kV A and $S_2 = 2$ kV A for inverters 1 and 2 respectively. It is expected that $P_2 = 2P_1$ and $Q_2 = 2Q_1$. Both inverters operate with a switching frequency of 15 kHz and the line frequency of the system is 50 Hz. The rated voltage of the inverters is $E^* = 230$ V and $K_e = 10$. The filter inductors are $L_1 = L_2 = 2.35$ mH with a parasitic resistance $R_1 = R_2 = 0.9\,\Omega$ and the filter capacitors are $C_1 = C_2 = 28\,\mu$F with parasitic resistance $r_{C1} = r_{C2} = 100\,\text{M}\Omega$. According to The grid code (2010), the desired voltage drop ratio is chosen as $\frac{n_i S_i^*}{K_e E^*} = 0.25\%$ and the frequency drop ratio is chosen $\frac{m_i S_i^*}{\omega^*} = 0.1\%$. Therefore, the droop coefficients are calculated as $n_1 = 0.0058$, $n_2 = 0.0029$, $m_1 = 3.1416 \cdot 10^{-4}$ and $m_2 = 1.5708 \cdot 10^{-4}$. Assume the parameter p is chosen as 0.2. The parameter c is determined according to (32) and the rest of the controller parameters are chosen as $k_E = k_z = 10$.

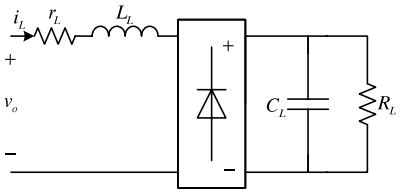

Fig. 9. Non-linear load.

The load considered is a non-linear load, as shown in Fig. 9, with $C_L = 330\ \mu\text{F}$, $R_L = 50\ \Omega$, $L_L = 2.35$ mH and a parasitic resistance $r_L = 0.9\ \Omega$, where the load resistance R_L changes to 100 Ω at the time instant $t = 8$ s. This nonlinear load is commonly used in industry and is a special case of a controlled rectifier as noted in Karagiannis et al. (2003), with the dynamic load equations satisfying (2).

Figs. 10 and 11 illustrate the time response of the parallelled inverters for the BDC and the RDC case respectively. Comparing Fig. 10(a) with Fig. 11(a), it is clear that both controllers achieve accurate sharing of the real and the reactive power respectively, proportional to the inverter ratings. This underlines their advantage over the conventional droop control techniques. Additionally, as it can be observed, the BDC achieves faster regulation at the desired steady-state values. This is due to the tuning of the parameter c which is larger at the beginning and reduces as the system approaches the desired equilibrium point. At the time instant $t = 8$ s, the load resistance R_L at the output of the load changes from 50 Ω to 100 Ω which forces both the real and the reactive power of each inverter to change. However, $P_2 = 2P_1$ and $Q_2 = 2Q_1$ are still maintained at the steady state. Note that, at the steady state, the BDC performance coincides with the RDC as it can be verified from the steady-state responses of the load voltage v_o and the inverter currents i_1, i_2 given in Fig. 10(b) and Fig. 11(b) respectively. This verifies the fact that the proposed method keeps the RDC theory intact. For the BDC, Fig. 10(c) shows that the controller states E_1 and E_{q1} travel along the circle on the $E_1 - E_{q1}$ plane at the origin with radius equal to $V_1 = (1 + p)\, E^* = 276$ V. The controller states stay always in the first quadrant and they converge to the desired steady-state values corresponding to the specific equilibrium point on the circle. In the same figure, the response of the controller states z_1 and z_{q1} on the z_1–z_{q1} plane is also presented. They travel clockwise on a circle at the origin with radius equal to 1 with angular velocity $\dot{\theta}$. This verifies the controller operation as described in Section 3.1 and consequently the stability analysis presented in Section 3.2.

5. Conclusions

In this paper, a bounded droop controller has been proposed to guarantee the stability of parallel-operated inverter systems in the sense of boundedness, while achieving accurate load sharing. In addition to maintaining the theory of the RDC, the BDC also introduces a bounded characteristic for the control output. An extended analysis using the small-gain theorem has been presented to certify that the proposed bounded control scheme guarantees the stability of the closed-loop system in the sense of boundedness independently from the type of the load (linear or non-linear). The controller structure has been further modified to increase its robustness to numerical errors and external disturbances by forming an attractive oscillator scheme. Real-time simulation results of two parallel single-phase inverters feeding a non-linear load have verified the proposed BDC.

An important issue in parallel operated inverters is the existence of the desired equilibrium point. Several researchers have provided conditions of existence of this equilibrium (Schiffer et al., 2014; Simpson-Porco et al., 2013) under the assumption of lossless microgrids and linear load description. The conditions of existence of the desired equilibrium in the general plant description described in this paper and the droop controller operation under undesired phenomena that may affect the equilibrium point are left for future research.

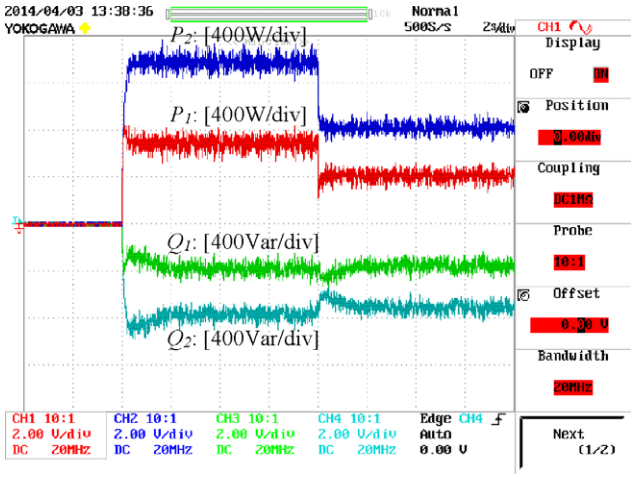

(a) Real and reactive power.

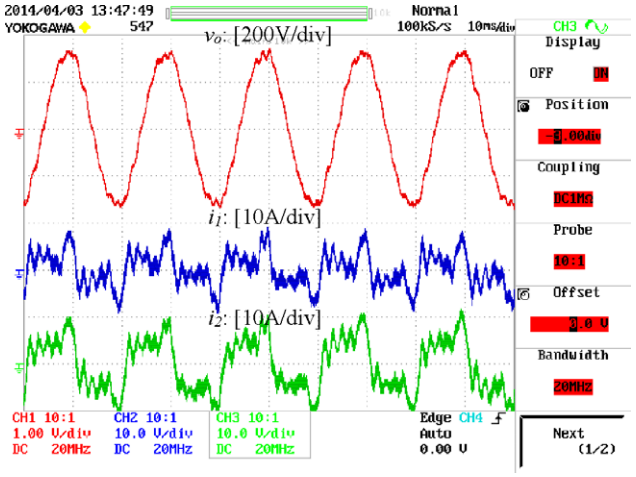

(b) Load voltage and inverter currents.

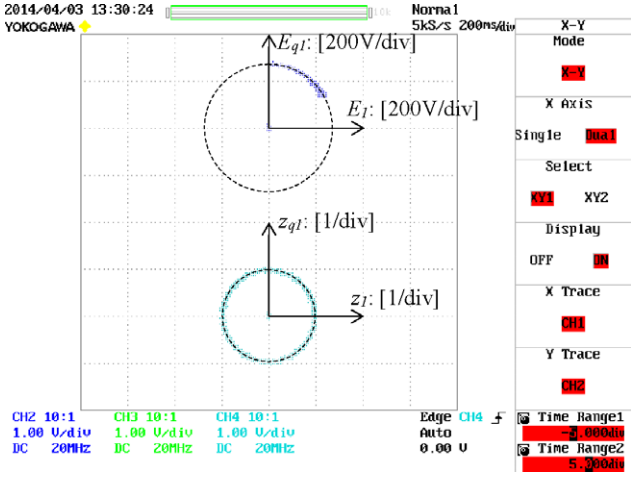

(c) Controller states on the $E_1 - E_{q1}$ and $z_1 - z_{q1}$ plane.

Fig. 10. Real-time simulation results using the BDC.

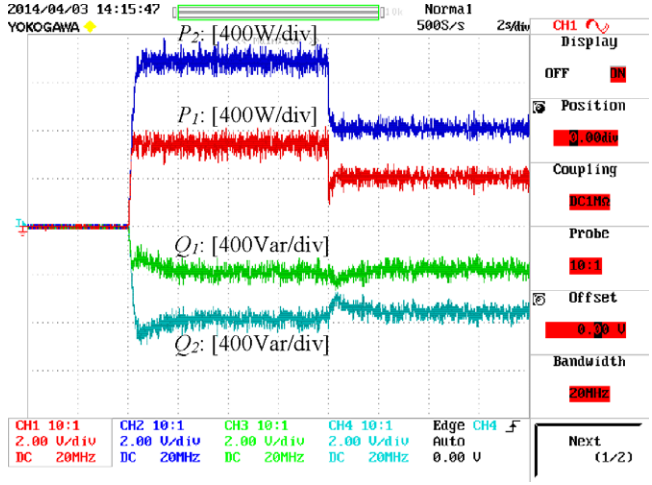

(a) Real and reactive power.

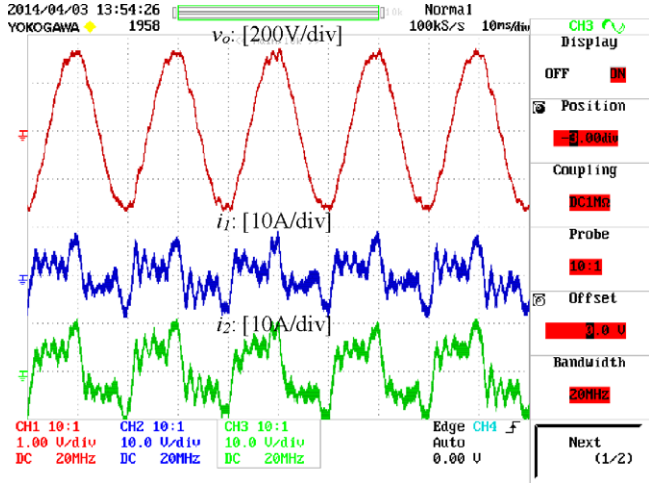

(b) Load voltage and inverter currents.

Fig. 11. Real-time simulation results using the RDC.

References

Barklund, E., Pogaku, N., Prodanovic, M., Hernandez-Aramburo, C., & Green, T. C. (2008). Energy management in autonomous microgrid using stability-constrained droop control of inverters. *IEEE Transactions on Power Electronics*, *23*(5), 2346–2352.

Chandorkar, M. C., Divan, D. M., & Adapa, R. (1993). Control of parallel connected inverters in standalone AC supply systems. *IEEE Transactions on Industry Applications*, *29*(1), 136–143.

Coelho, E. A. A., Cortizo, P. C., & Garcia, P. F. D. (2002). Small-signal stability for parallel-connected inverters in stand-alone AC supply systems. *IEEE Transactions on Industry Applications*, *38*(2), 533–542.

Guerrero, J. M., Berbel, N., de Vicuna, L. G., Matas, J., Miret, J., & Castilla, M. (2006). Droop control method for the parallel operation of online uninterruptible power systems using resistive output impedance. In *Proc. of the 21st IEEE applied power electronics conference and exposition* (pp. 1716–1722).

Guerrero, J., Chandorkar, Mukul, Lee, T., & Loh, P. (2013). Advanced control architectures for intelligent microgrids—part I: decentralized and hierarchical control. *IEEE Transactions on Industrial Electronics*, *60*(4), 1254–1262.

Guerrero, J. M., de Vicuna, L. G., Matas, J., Castilla, M., & Miret, J. (2005). Output impedance design of parallel-connected UPS inverters with wireless load-sharing control. *IEEE Transactions on Industrial Electronics*, *52*(4), 1126–1135.

Guerrero, J., Loh, P., Lee, T., & Chandorkar, Mukul (2013). Advanced control architectures for intelligent microgrids—part II: power quality, energy storage, and AC/DC microgrids. *IEEE Transactions on Industrial Electronics*, *60*(4), 1263–1270.

Guerrero, J. M., Matas, J., de Vicuna, L. G., Castilla, M., & Miret, J. (2007). Decentralized control for parallel operation of distributed generation inverters using resistive output impedance. *IEEE Transactions on Industrial Electronics*, *54*(2), 994–1004.

Guerrero, J. M., Vasquez, J. C., Matas, J., Castilla, M., & de Vicuna, L. G. (2009). Control strategy for flexible microgrid based on parallel line-interactive UPS systems. *IEEE Transactions on Industrial Electronics*, *56*(3), 726–736.

Guerrero, J. M., Vasquez, J. C., Matas, J., Garcia de Vicuna, L., & Castilla, M. (2011). Hierarchical control of droop-controlled AC and DC microgrids—a general approach towards standardization. *IEEE Transactions on Industrial Electronics*, *58*(1), 158–172.

Iyer, S. V., Belur, M. N., & Chandorkar, M. C. (2010). A generalized computational method to determine stability of a multi-inverter microgrid. *IEEE Transactions on Power Electronics*, *25*(9), 2420–2432.

Karagiannis, D., Mendes, E., Astolfi, A., & Ortega, R. (2003). An experimental comparison of several PWM controllers for a single-phase AC-DC converter. *IEEE Transactions on Control Systems Technology*, *11*(6), 940–947.

Khalil, Hassan K. (2001). *Nonlinear systems*. Prentice Hall.

Konstantopoulos, G. C., & Alexandridis, A. T. (2013). Generalized nonlinear stabilizing controllers for Hamiltonian-passive systems with switching devices. *IEEE Transactions on Control Systems Technology*, *21*(4), 1479–1488.

Li, Y. W., & Kao, C.-N. (2009). An accurate power control strategy for power-electronics-interfaced distributed generation units operating in a low-voltage multibus microgrid. *IEEE Transactions on Power Electronics*, *24*(12), 2977–2988.

Majumder, R., Chaudhuri, B., Ghosh, A., Ledwich, G., & Zare, F. (2010). Improvement of stability and load sharing in an autonomous microgrid using supplementary droop control loop. *IEEE Transactions on Power Systems*, *25*(2), 796–808.

Marwali, M. N., Jung, J.-W., & Keyhani, A. (2007). Stability analysis of load sharing control for distributed generation systems. *IEEE Transactions on Energy Conversion*, *22*(3), 737–745.

Mohamed, Y., & El-Saadany, E. F. (2008). Adaptive decentralized droop controller to preserve power sharing stability of paralleled inverters in distributed generation microgrids. *IEEE Transactions on Power Electronics*, *23*(6), 2806–2816.

The grid code, (2010). *Technical report*. National Grid Electricity Transmission PLC.

Ortega, R., Loria, Antonio, Nicklasson, Per Johan, & Sira-Ramirez, Hebertt (1998). *Passivity-based control of Euler–Lagrange systems, mechanical, electrical and electromechanical applications*. Great Britain: Springer-Verlag.

Sao, C. K., & Lehn, P. W. (2005). Autonomous load sharing of voltage source converters. *IEEE Transactions on Power Delivery*, *20*(2), 1009–1016.

Schiffer, J., Ortega, R., Astolfi, A., Raisch, J., & Sezi, T. (2014). Conditions for stability of droop-controlled inverter-based microgrids. *Automatica*, *50*(10), 2457–2469.

Simpson-Porco, J. W., Dörfler, F., & Bullo, F. (2013). Synchronization and power sharing for droop-controlled inverters in islanded microgrids. *Automatica*, *49*(9), 2603–2611.

Tuladhar, A., Jin, H., Unger, T., & Mauch, K. (1997). Parallel operation of single phase inverter modules with no control interconnections. In *Proc. of the 12th IEEE applied power electronics conference and exposition* (pp. 94–100).

Weiss, G., Zhong, Q.-C., Green, T., & Liang, J. (2004). H^∞ repetitive control of DC-AC converters in micro-grids. *IEEE Transactions on Power Electronics*, *19*(1), 219–230.

Zhong, Q.-C. (2013). Robust droop controller for accurate proportional load sharing among inverters operated in parallel. *IEEE Transactions on Industrial Electronics*, *60*(4), 1281–1290.

Zhong, Q.-C., & Hornik, T. (2013). *Control of power inverters in renewable energy and smart grid integration*. Wiley-IEEE Press.

George C. Konstantopoulos received his Diploma and Ph.D. in Electrical and Computer Engineering from the University of Patras, Greece, in 2008 and 2012, respectively. Since 2013, he has been with the Department of Automatic Control and Systems Engineering, The University of Sheffield, UK, where he is currently a Research Fellow. His current research interests include nonlinear modelling, control and stability analysis of power converter and electric machine systems with emphasis in microgrid operation, renewable energy systems and motor drives.

Qing-Chang Zhong received the Ph.D. degree in control theory and engineering from Shanghai Jiao Tong University in 2000, and the Ph.D. degree in control and power engineering from Imperial College London in 2004.

He holds the Max McGraw Endowed Chair Professor in Energy and Power Engineering at Illinois Institute of Technology, Chicago, USA, and a Research Chair at The University of Sheffield, UK. He is a Distinguished Lecturer of IEEE Power Electronics Society and the UK Representative to the European Control Association. He (co-)authored three research monographs, including Control of Power Inverters in Renewable Energy and Smart Grid Integration (Wiley-IEEE Press, 2013) and Robust Control of Time-delay Systems (Springer, 2006), and proposed the architecture for next-generation smart grids to unify the interface of all players with the grid through the synchronisation mechanism of conventional synchronous machines. He serves as an Associate Editor for IEEE Transactions on Automatic Control/Power Electronics/Industrial Electronics/Control Systems Technology, IEEE Access, IEEE Journal of Emerging and Selected Topics in Power Electronics, and European Journal of Control. His research focuses on advanced control theory and its

applications to various sectors including power and energy engineering, chemical engineering and mechatronics.

Beibei Ren received the B. Eng. degree in the Mechanical & Electronic Engineering and the M. Eng. degree in Automation from Xidian University, Xi'an, China, in 2001 and in 2004, respectively, and the Ph.D. degree in the Electrical and Computer Engineering from the National University of Singapore, Singapore, in 2010. From 2010 to 2013, she was a postdoctoral scholar in the Department of Mechanical & Aerospace Engineering, University of California, San Diego, CA, USA. Since 2013, she has been with the Department of Mechanical Engineering, Texas Tech University, Lubbock, TX, USA, as an Assistant Professor. Her current research interests include adaptive control, robust control, distributed parameter systems, extremum seeking and their applications.

Miroslav Krstic holds the Alspach endowed chair and is the founding director of the Cymer Center for Control Systems and Dynamics at UC San Diego. He also serves as Associate Vice Chancellor for Research at UCSD. As a graduate student, Krstic won the UC Santa Barbara best dissertation award and student best paper awards at CDC and ACC. Krstic is a Fellow of IEEE, IFAC, ASME, and IET (UK), and a Distinguished Visiting Fellow of the Royal Academy of Engineering. He has received the PECASE, NSF Career, and ONR Young Investigator awards, the Axelby and Schuck paper prizes, the Chestnut textbook prize, and the first UCSD Research Award given to an engineer. Krstic has held the Springer Visiting Professorship at UC Berkeley. He serves as a Senior Editor in IEEE Transactions on Automatic Control and Automatica, as editor of two Springer book series, and has served as Vice President for Technical Activities of the IEEE Control Systems Society and as chair of the IEEE CSS Fellow Committee. Krstic has co-authored ten books on adaptive, nonlinear, and stochastic control, extremum seeking, control of PDE systems including turbulent flows, and control of delay systems.